Earthq Eng & Eng Vib (2021) 20: 863-876 **DOI**: https://doi.org/10.1007/s11803-021-2059-y

Experimental *p-y* curves for liquefied soils from centrifuge tests

Suresh R. Dash[1†] and Subhamoy Bhattacharya[2‡]

1. *School of Infrastructure, Indian Institute of Technology Bhubaneswar, India*

2. *Department of Civil and Environmental Engineering, University of Surrey, UK*

Abstract: The present study aims to obtain *p-y* curves (Winkler spring properties for lateral pile-soil interaction) for liquefied soil from 12 comprehensive centrifuge test cases where pile groups were embedded in liquefiable soil. The *p-y* curve for fully liquefied soil is back-calculated from the dynamic centrifuge test data using a numerical procedure from the recorded soil response and strain records from the instrumented pile. The *p-y* curves were obtained for two ground conditions: (a) lateral spreading of liquefied soil, and (b) liquefied soil in level ground. These ground conditions are simulated in the model by having collapsing and non-collapsing intermittent boundaries, which are modelled as quay walls. The *p-y* curves back-calculated from the centrifuge tests are compared with representative reduced API *p-y* curves for liquefied soils (known as *p*-multiplier). The response of *p-y* curves at full liquefaction is presented and critical observations of lateral pile-soil interaction are discussed. Based on the results of these model tests, guidance for the construction of *p-y* curves for use in engineering practice is also provided.

Keywords: liquefaction; pile foundation; *p-y* curve; centrifuge test

1 Introduction

The beam on nonlinear Winkler foundation (BNWF) model is extensively used in practice for pseudo-static analysis of piles due to its simplicity, mathematical convenience, and ability to incorporate nonlinearity (Finn, 2005; Thavaraj *et al*., 2010; Madabhushi *et al.*, 2009; Bhattacharya *et al.*, 2019). In a BNWF model, the lateral-pile-soil-interaction (LPSI) is usually modelled as a lumped soil spring with a nonlinear backbone curve. These nonlinear backbone curves are also known as *p-y* curves, where '*p*' refers to the lateral soil pressure per unit length of the pile, and the '*y*' refers to the relative pile-soil displacement (see Fig. 1).

1.1 Current understanding of the *p-y* curves in liquefied soil

The *p-y* curve for normal soil condition (i.e., non-liquefied soil in this context) is well understood and used in practice with confidence (for example, see API (2014) and JRA (2002), where the procedure for constructing *p-y* curves for various types of soils is provided). During liquefaction, the soil changes its solid-state to a fluid-state and many of the index properties of the soil also change. The interaction between the pile and the liquefied soil is indeed complicated. Traditionally, engineers use simple solutions to tackle this complex situation and use a reduction factor (α) over the soil resistance (p) for liquefied soil (AIJ, 2001; Brandenberg, 2005), as shown schematically in Fig. 1. This reduction factor depends on various field conditions such as degree of liquefaction, depth of liquefied soil versus depth of non-liquefied crust, etc. A collation of α values available in the literature is given in Dash *et al*. (2008). This way of modelling *p-y* curves by applying a reduction factor over the *p-y* curve of non-liquefied soil is being used by many researchers, including some recent studies (see Janalizadeh and Zahmatkesh (2015), Zhang and Yang (2018)). As shown in Fig. 1, the *p-y* curve used in practice for liquefied soil is merely a reduced strength *p-y* curve obtained from the *p-y* curve of non-liquefied soil, keeping the ultimate displacement value constant. Further details of the shape of experimental *p-y* curves and their importance for liquefied and non-liquefied soils can be found in Dash *et al.* (2008), Gerolymos (2009), Dash (2010), Bouzid *et al.* (2013), Lombardi *et al.* (2017) and Dash *et al.* (2017).

1.2 Experimental observation of the *p-y* curves in liquefied soil

The reduced strength *p-y* curve, as described above, still keeps a high value of initial stiffness. In contrast, many recent experimental observations (for example, Wilson *et al*., 2000; Rollins *et al*., 2005; Mohanty *et al.*, 2021) suggest that the shape of the liquefied soil is

Correspondence to: Suresh R. Dash, School of Infrastructure, Indian Institute of Technology Bhubaneswar, India
Tel: +91-674 713 6638
E-mail: srdash@iitbbs.ac.in
[†]Assistant Professor; [‡]Professor

Received August 14, 2020; **Accepted** March 21, 2021

like an S-curve, having negligible stiffness at the initial straining phase (see Fig. 1). The lack of initial stiffness of the liquefied soil will increase the P-delta effect in the small-amplitude vibration and may promote buckling mode of failure of piles, which might not be captured in the numerical study if the present *p-y* curve model is used. Readers are referred to Chapter 5 of Bhattacharya *et al*. (2019) for further details.

With reference to the above discussion, the shape and magnitude of *p-y* curves are studied herein using 12 comprehensive centrifuge test data of pile group responses in liquefiable soils. The *p-y* curves for liquefied soils are back-calculated from the recorded strain values of the pile. The calculated *p-y* curves are also compared with the available API type *p-y* curves, and the observations are discussed. All the analyses of the test cases are carried out on a prototype scale unless otherwise specified.

2 Description of centrifuge model setup

In this study, test data from eight centrifuge tests carried out (16 pile groups) at Shimizu Corporation, Japan (Tazoh *et al.*, 2008) have been taken for a detailed study. The raw data was provided personally by Dr. Takashi Tazoh in 2008, when he was the deputy director of Institute of Technology, Shimizu Corporation, Tokyo, Japan. The tests were conducted at 1:30 scale (i.e., at 30 times earth′s gravity (g)). The details of the centrifuge facility used can be found in Sato (1994). The models were tested in a laminar box of dimensions 805 mm long, 475 mm wide and 324 mm high. The models were subjected to a varying magnitude base acceleration of a 60 Hz sine wave (2 Hz at prototype scale). Figure 2 shows the input motion used in the test and the pore water pressure generation in the soil at two depths in the prototype scale. The maximum value of the pore water pressure should be equal to the overburden pressure at full liquefaction. However, the observance of slight overshooting of this value in Fig. 2 can be attributed as follows: (1) the actual effective stress at the measuring location might be more than the calculated value due to densification, and/or (2) settlement/dislocation of the pore water pressure sensor during the test. A superstructure mass was also added to the pile head to apply a reasonable amount of axial load to the piles.

2.1 Test layout

Eight experimental test sets are used in the current study (see Table 1, CT*i*-A or B, i = 1 to 8). Each experimental setup (see Fig. 3) consisted of two pile groups (denoted as A or B), separated by a rigid partition wall. Each pile group was composed of four piles fixed to the base of the container. At one end of the laminar box, the soil and water were separated by a stiff quay wall of 10 mm (30 cm in prototype scale) thick aluminium sheet. The quay wall was held in position by soil fill on both sides, and free at the bottom and was stable at the start of the test. The case where the quay wall collapsed (e.g., CT1-B) can be considered as a case of lateral spreading, whereas the liquefaction in the level ground can be represented when the quay wall did not collapse (e.g., CT1-A). This kind of setup was beneficial in modelling both pile groups with the required soil/structural parameter variation while keeping all other model parameters the same. In each test, both pile groups (A and B) were subjected to nearly identical conditions with respect to input motions and soil liquefaction. Hence, a total of 16 pile groups were tested. As this investigation is limited to vertical piles only, four pile groups having

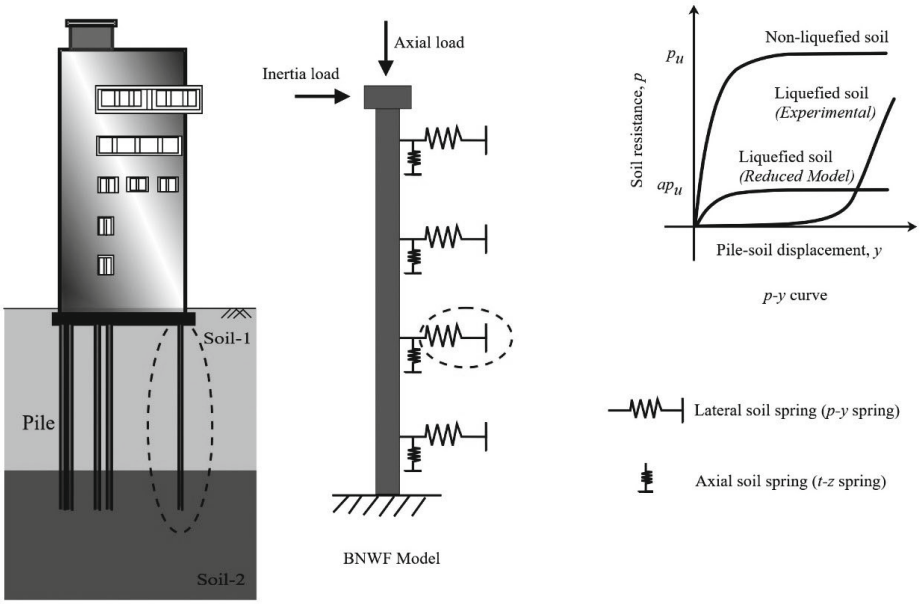

Fig. 1 Pseudo-static BNWF model of pile-soil interaction (PSI) study

batter piles (CT5-B, CT6-B, CT7-B, and CT8-B) were excluded from this study. For ease of representation, each pile group is treated separately. The details of the 12 pile groups studied are presented in Tables 1 and 2.

2.2 Model details

Figure 4 shows a schematic of the test setup for 12 pile groups according to Tables 1 and 2. The pile groups were divided into two major categories depending on the quay wall fixity and three layout types according to the number of data acquisition locations, as detailed in Table 2. The structural properties of the model piles are given in Table 3. Both the front and back sides of two piles in the pile group were instrumented with strain gauges at the locations shown in Fig. 4. Two types of soil (Silica sand and Toyoura sand) were used in four layers in the model, whose geotechnical properties are presented in Table 4. High viscosity silicone oil was used as the pore fluid and its viscosity was 30 times that of the water to satisfy scaling requirements for the diffusion process. The water table in various centrifuge models is shown in Fig. 4. Table 5 presents the scaling laws used while converting the model scale responses of the pile and soil to prototype scale.

3 Procedure of estimating the *p-y* curve

As mentioned earlier, the *p-y* curve is the representation of lateral pile-soil interaction, where *p* refers to the soil resistance and *y* refers to relative pile-soil displacement. This relative pile-soil displacement is the difference between pile displacement (y_p) and soil displacement near the pile (y_s) (Eq. (1)).

$$y = y_p - y_s \tag{1}$$

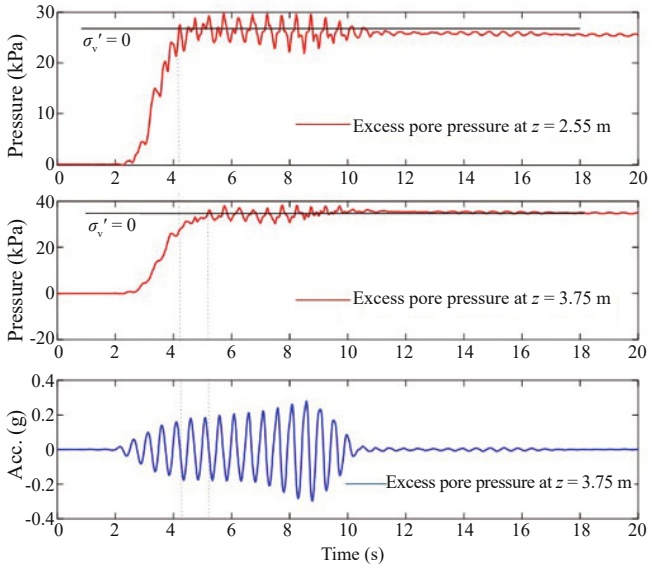

Fig. 2 Input Motion and pore water pressure generation in the soil in prototype scale (z is the distance from top of the soil layer)

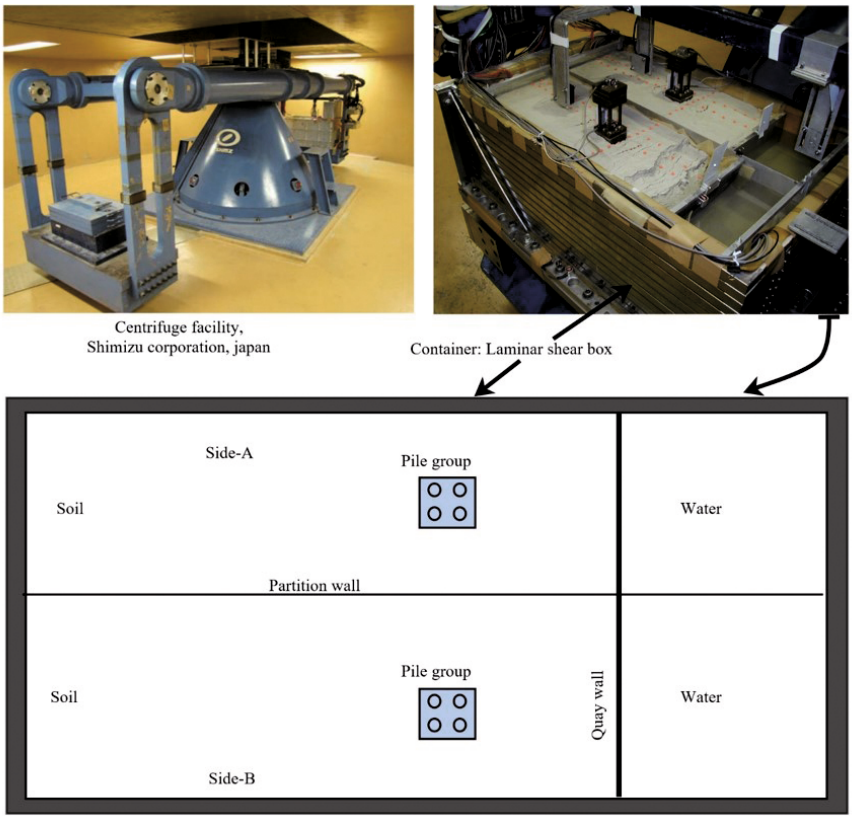

Fig. 3 Typical test setup of dynamic centrifuge testing

Table 1 Description of centrifuge tests used in the present model study

Test No.	Pile Group	Description (Refer to Fig. 4 for schematic illustration of these test setups)
CT1	A	Fixed end quay wall. X2 = 200 mm, quay wall did not collapse during the test.
	B	Free end quay wall. X2 = 200 mm, quay wall collapsed during the test.
CT2	A	Fixed end quay wall. X2 = 100 mm, quay wall did not collapse during the test.
	B	Free end quay wall. X2 = 100 mm, quay wall collapsed during the test.
CT3	A	Fixed end quay wall. X2 = 50 mm, quay wall did not collapse during the test.
	B	Free end quay wall. X2 = 50 mm, quay wall collapsed during the test.
CT4	A	Free end quay wall. X2 = 50 mm, quay wall collapsed during the test.
	B	Free end quay wall. X2 = 100 mm, quay wall collapsed during the test.
CT5	A	Free end quay wall. X2 = 200 mm, quay wall collapsed during the test.
	B	Batter pile group (Not included in the present study)
CT6	A	Free end quay wall. X2 = 100 mm, quay wall collapsed during the test.
	B	Batter pile group (Not included in the present study)
CT7	A	Free end quay wall. X2 = 50 mm, quay wall collapsed during the test.
	B	Batter pile group (Not included in the present study)
CT8	A	Repetition of CT7-A, quay wall collapsed during the test.
	B	Batter pile group (Not included in the present study)

Table 2 Two major field conditions simulated in the pile group study

Field conditions simulated	Quay wall fixity at base	Pile groups in the specified category	Measurements locations	Test layout according to:
Non-spreading liquefied ground	Fixed base quay wall	CT1-A CT2-A CT3-A	Strain measurement at four depths, soil acceleration at two depths	Fig. 4(a)
lateral spreading liquefied ground	Free base quay wall	CT1-B CT2-B CT3-B CT4-A, CT4-B	Strain measurement at four depths, soil acceleration at two depths	Fig. 4(b)
		CT5-A CT6-A CT7-A CT8-A	Strain measurement at five depths, soil acceleration at three depths	Fig. 4(c)

Table 3 Structural properties of the model pile

Item	Value
Material	Stainless steel
Pile outside diameter, D_o	10 mm
Wall thickness	0.2 mm
Moment of inertia of pile, I_p	73.95 mm^4
Young′s modulus, E_p	210 GPa
Yield moment capacity, M_y	3845 N·mm (104 kN·m in prototype scale)

Table 4 Geotechnical properties of the sand used in the test

Symbol	Unit	Soil 1	Soil 2	Soil 3	Soil 4
		Unsaturated silica sand No. 8	Saturated silica sand No. 8	Saturated Toyoura sand	Saturated silica sand No. 3
e_{max}	--	1.385	1.385	0.951	0.974
e_{min}	--	0.797	0.797	0.593	0.654
D_r	%	50	50	90	90
γ'	kN/m^3	7.652	7.652	9.908	9.496
γ_t	kN/m^3	12.851	--	--	--
S_r	%	10	100	100	100

e_{max}= maximum void ratio, e_{min}= minimum void ratio, D_r = relative density, γ' = effective unit weight of soil, γ_t = dry unit weight of soil, S_r= saturation ratio.

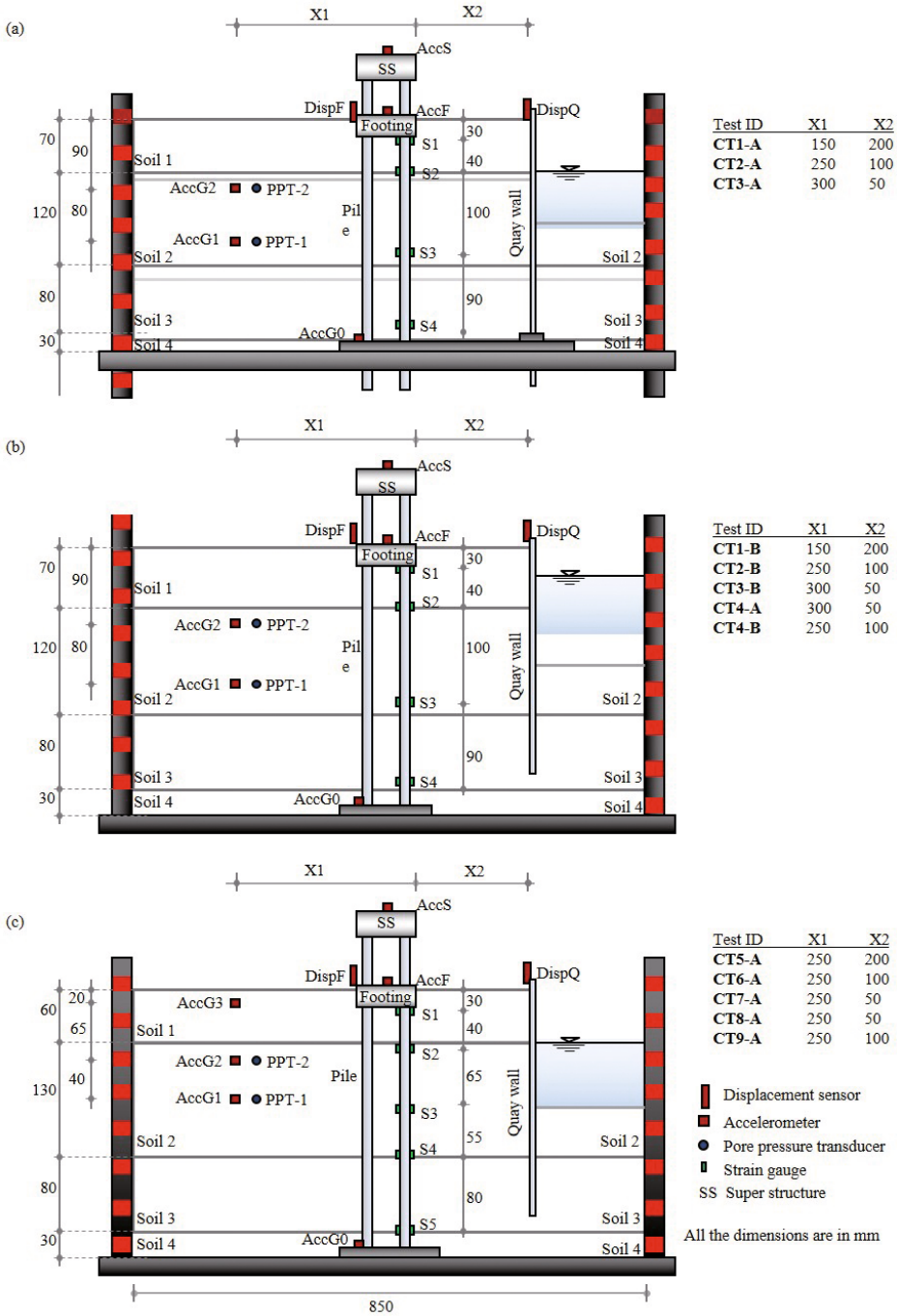

Fig. 4 Schematic of test layout and instrumentation

Table 5 Scaling laws for centrifuge model tested at *n*-g

Parameters	Unit	Model / prototype ratio
Stress (σ)	$ML^{-1}T^{-2}$	1
Strain (ε)	-	1
Length	L	$1/n$
Time (dynamic)	T	$1/n$
Acceleration	LT^{-2}	n
Pile bending stiffness (E_pI_p)	$ML^{-3}T^{-2}$	$1/n^4$
Natural frequency (f_n)	T^{-1}	$1/n$

The p and y_p can be back-calculated from the recorded bending strain (ε_b) of the pile using the equations of beam bending. The curvature and bending moment in a pile can be directly computed from the recorded pile bending strain by using Eqs. (2) and (3). The pile deflection, y_p, can then be computed by integrating the bending moment profile of the pile twice with respect to depth, z, and dividing that by E_pI_p (Eq.(4)). Similarly, p can be calculated by double differentiating the bending moment profile with depth x (Eq. (5)).

$$\text{Curvature} = \frac{1}{\rho_{\mathrm{p}}} = \frac{\varepsilon_{\mathrm{b}}}{D/2} \tag{2}$$

$$\text{Bending moment} = M = E_{\mathrm{p}} I_{\mathrm{p}} \frac{1}{\rho_{\mathrm{p}}} \tag{3}$$

$$\text{Pile deflection} = y_{\mathrm{p}} = \frac{1}{E_{\mathrm{p}} I_{\mathrm{P}}} \iint M \mathrm{d}x \tag{4}$$

$$\text{Soil resistance} = p = \frac{\mathrm{d}}{\mathrm{d}x}\left(\frac{\mathrm{d}}{\mathrm{d}x} M\right) \tag{5}$$

where D is the diameter and $E_{\mathrm{p}} I_{\mathrm{p}}$ is the bending stiffness of the pile.

The soil displacement near to the pile (y_{s}) was estimated separately from the measured soil acceleration and quay wall displacement data. As the pile has not undergone any permanent deformation as per the post-test observation, a linear elastic behavior of the piles was considered.

4 Signal processing of the recorded data

The estimation of *p-y* curve, as described in the previous section, involved three major steps:

1. Double integration of bending moment along the pile to obtain pile deflection.

2. Double differentiation of bending moment along the pile to obtain soil resistance.

3. Double integration of soil acceleration to get displacement time history of the free-field soil.

In a continuous signal, the integration is sensitive to low-frequency data and the differentiation is sensitive to high-frequency data. Hence, it is important to filter both high and low-frequency noise from the signal to obtain a reliable estimate of *p* and *y* during the integration and differentiation of the data. As pointed out by many researchers (e.g., Han, 2003; Park *et al*., 2005; Chanerley and Alexander, 2007), inappropriate filtering of the recorded data may greatly affect the estimated response of the system. A detailed sensitivity analysis was therefore performed to arrive at a reliable procedure of filtering the measured unfiltered signal prior to the back-calculation of the *p-y* curves. The original base acceleration and its Welch power spectral density for the tests have shown the presence of both high and low-frequency noise apart from the forcing frequency of 2 Hz (60 Hz in model scale). The fundamental frequency of the soil-pile-footing-structure (SPFS) system was varying during the test as the soil liquefied. The first fundamental frequency of the SPFS system was estimated by dynamic amplification factor analysis using the acceleration time history recorded at the top of the footing with respect to the input base acceleration. The analysis showed that the fundamental frequency of the SPFS systems during the test was roughly varying from 7 Hz (before liquefaction) to 1 Hz (at full liquefaction) for all the cases considered.

Hence, a digital band-pass filter was designed to remove the unwanted signal from the measured data leaving the signals with the frequencies of interest. Finally, an 8th order band-pass Butterworth filter was chosen with the frequency passband of 0.4 Hz – 10 Hz, which provided consistent results for all the test cases. The filtering of data was carried out using the MATLAB "filtfilt" command to obtain a zero-phase distortion during filtering.

5 Dynamic bending moment and its curve fitting

From the measured strain in the pile, bending strain is estimated and then filtered to obtain its dynamic component. Using beam bending equations (Eqs. (2) and (3)), bending moments in the pile at the strain measurement points were obtained. To be able to carry out the integration and differentiation of the bending moment in the pile for estimating *p* and *y*, an appropriate curve-fitting method was sought.

One of the most common ways in which many researchers use to fit the discrete bending moment data to obtain a bending moment profile along the pile length is by using interpolation functions. The interpolation functions can be a continuous polynomial (Matlock and Ripperger, 1956; Rollins *et al*., 2005) or a segmented cubic spline (as used by Dou and Byrne (1996)) or a weighted residual method (as used by Wilson (1998)) or an average representation of various curve fitting values including polynomial function, cubic spline function and Loess function (Jeanjean, 2009).

In the present case, to arrive at the best curve fitting option, four different methods were studied in detail where the depth was taken as the variable *x*. Figure 5 plots the discrete bending moment values and the curve fitted for the above mentioned four fitting methods, for the test case CT6-A, as a representative case. All of the methods fit the bending moment data points quite well in the liquefied soil zone, 1.8 m to 5.7 m, where the final *p-y* curves were back-calculated. The bending moment fitting and its computed values yield a similar profile irrespective of the time step of consideration. Though all the methods of curve fitting gave similar results for bending moment, shear force and slope, the deflection profile obtained varied greatly between the methods, which may be attributed to the order of the polynomial fits. Hence, the calculations for '*p*' and '*y*' were carried out with all four methods of curve fitting and the results are compared. For the tests where the strain measurements were available only at four discrete locations (e.g., CT1, CT2, CT3 and CT4), the order of the polynomial fits was reduced by one.

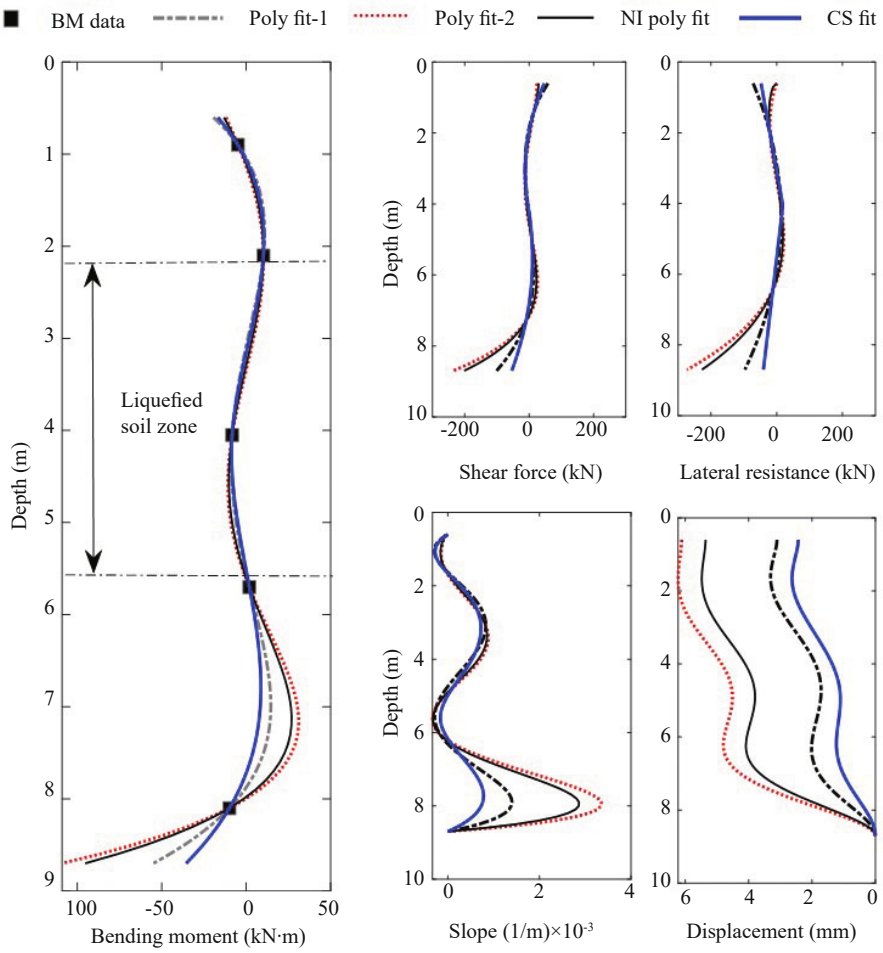

Fig. 5 Bending moment and its fitted curve at t = 6 s (for case CT6-A) by four different fits, and the derived shear force, lateral resistance, slope, and pile displacement. (Note: poly fit-1: $M = A + Bx + Cx^2 + Dx^3 + Ex^4$; poly fit-2: $M = A + Bx + Cx^3 + Dx^4 + Ex^5$; NI poly fit: $M = A + Bx + Cx^{2.5} + Dx^3 + Ex^4$; CS fit: cubic spline)

6 Back-calculation of *p-y* curves

6.1 Soil resistance, *p*

The fitted bending moment profile was double differentiated to obtain the lateral soil resistance (unit: force/length). Figure 6 shows the estimated lateral resistance from all four bending moment fits at three different depths (2.1 m, 4.05 m, and 5.7 m) for the representative case, CT6-A. Very good agreement between different fit methods was obtained at shallow depths, but at greater depths, the results varied significantly. This poor agreement shows that the data did not uniquely fit the bending moment profile throughout the depth. However, at the depths of consideration, (i.e., the depth of liquefiable soil layer), the agreement between the results of different fitting methods is good, except for the Poly fit-1. The cubic spline fit (CS-fit) provided a reasonably better curve fit for all the test cases and when the data points were less, this method performed comparatively better than the other fitting methods. Hence, in the further presentation of the lateral resistance, the values obtained from the CS-fit method (a 3rd order piecewise polynomial curve fitting method) were used.

6.2 Pile deflection, y_p

Pile deflection was estimated by integrating the fitted bending moment profile twice. During the integration, slope and deflection of the pile tip were taken as zero as the boundary condition. The fitted profile was compared with the slope values at the pile head and was corrected for zero pile head slope. The pile deflections estimated from four bending moment fitting methods are presented in Fig. 6. Although the deflection pattern is similar, the magnitude varied between the methods. The CS-fit, which was chosen for the final representation of the soil resistance (p), gives a lower magnitude of deflection than the other three methods. For consistency in the evaluation of the *p-y* curve, the CS-fit method was also chosen to estimate y_p.

6.3 Free field soil displacement, y_{sf}

The time history of soil displacement was estimated by double integrating the free field acceleration measurements taken at the locations away from the pile group (see Fig. 4 for the locations of acceleration measurements AccG0, AccG1, AccG2, and AccG3). The acceleration data were filtered and integrated twice to give the soil displacement. Note that during the filtering process, the dynamic component of the displacement is well preserved; however, any permanent component of displacement, if actually present, is removed. Surface observation after the test (Tazoh *et al.*, 2008) suggests that the locations where free field measurements were taken did not experience any permanent ground deformation (i.e., no crack formation on the surface). Hence, the dynamic component computed here is taken with reasonable confidence in the calculation. As the integration of acceleration data gives absolute values of displacement, the displacement of soil with respect to the base of the container was obtained by subtracting the container base displacement from the estimated absolute soil displacement. As described earlier, the soil profile consists of four layers with both liquefied and non-liquefied soil. The soil displacement profile along the depth is assumed as a linear interpolation between the measurement points, but the value at the bottom of the liquefied layer is restricted to roughly about 1/3rd of the linear interpolated value to account for the continuity between the liquefied soil layer and its underlying stiffer non-liquefied soil layer.

6.4 Soil displacement near quay wall, y_q

The only measurement available near the quay wall was the movement of the top of the quay wall. The top 70 mm of the quay wall was free on one side and supporting the non-liquefied soil on the other side. Considering the quay wall as stiff, a linear deflection profile has been assumed for fixed and free end quay walls. The fixed end quay wall hardly had any deflection at its top. The soil near to the quay wall was assumed to deflect the same way as the quay wall, without any gap in between.

6.5 Soil displacement near the pile, y_s

Knowing the deflection profile of free field soil (y_{sf}) and the soil near the quay wall (y_q), the deflection profile of the soil near the pile was linearly interpolated, as shown in Eq. (6).

$$y_s = y_q - \frac{y_q - y_{sf}}{a+b} \times b \tag{6}$$

6.6 Relative pile-soil displacement, y

Once the soil deflection near the pile and the pile deflection are computed, the relative soil-pile deflection, y, was calculated for each time step by subtracting the soil deflection from pile deflection using Eq. (1). This relative pile-soil displacement profile is estimated at each time step for the full length of the test.

7 Representation of *p-y* curves

The estimation procedure of 'p' and 'y' has already been demonstrated in the previous section for the representative case CT6-A. The plot between p and y at each time step constructs a dynamic *p-y* curve. The *p-y* curve for all other cases was carried out with the same analysis procedure as described for the case CT6-A. Note that some cases may give an improved performance of *p-y* behavior if filtering parameters and bending moment curve fitting methods are tuned, but to have consistency among the test results, the same numerical procedure of data analysis was followed for all the test cases. The

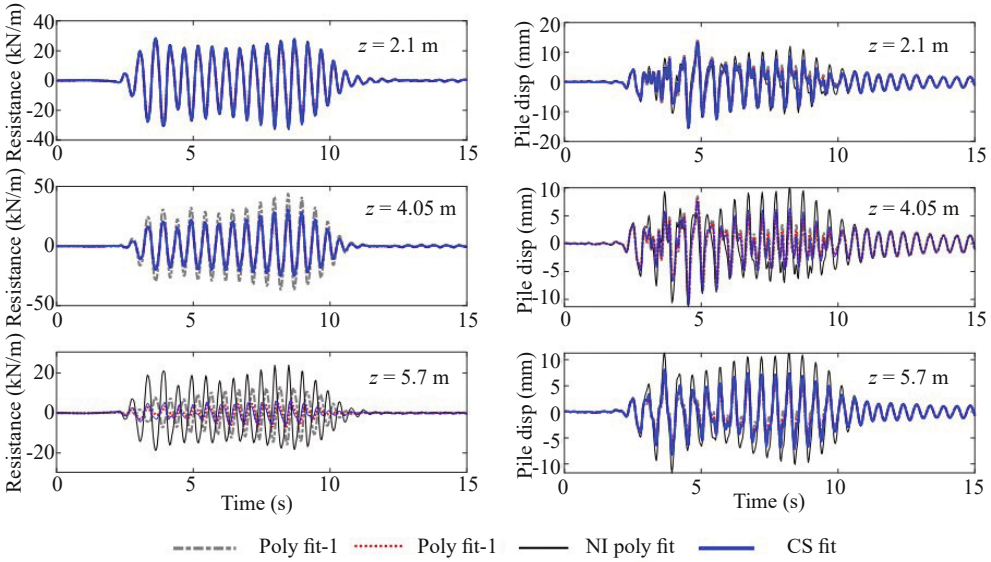

Fig. 6 Lateral soil resistance and pile displacement estimated for CT6-A at three different depths for various bending moment fits

back-calculated *p-y* curves were compared with API recommended monotonic *p-y* curves (API, 2014) for sand in non-liquefied conditions. The API curve was scaled down to 10% to obtain a reasonable comparison with the back-calculated *p-y* curve for liquefied soil within the scale of the axis, which is also one of the current practices of modelling *p-y* curves in liquefied soil as suggested by AIJ (2001). The *p-y* curves are plotted with normalized values of resistance and displacement.

7.1 *p-y* curves for no lateral spreading cases (level ground condition)

The test cases CT1-A, CT2-A and CT3-A had a non-failing quay wall at the end with no large lateral soil flow. Hence, these cases were considered as liquefiable soil without lateral spreading. Figure 7 shows the *p-y* curves estimated for these three cases at full liquefaction (6–10 s) at two depths (top and bottom of the liquefied

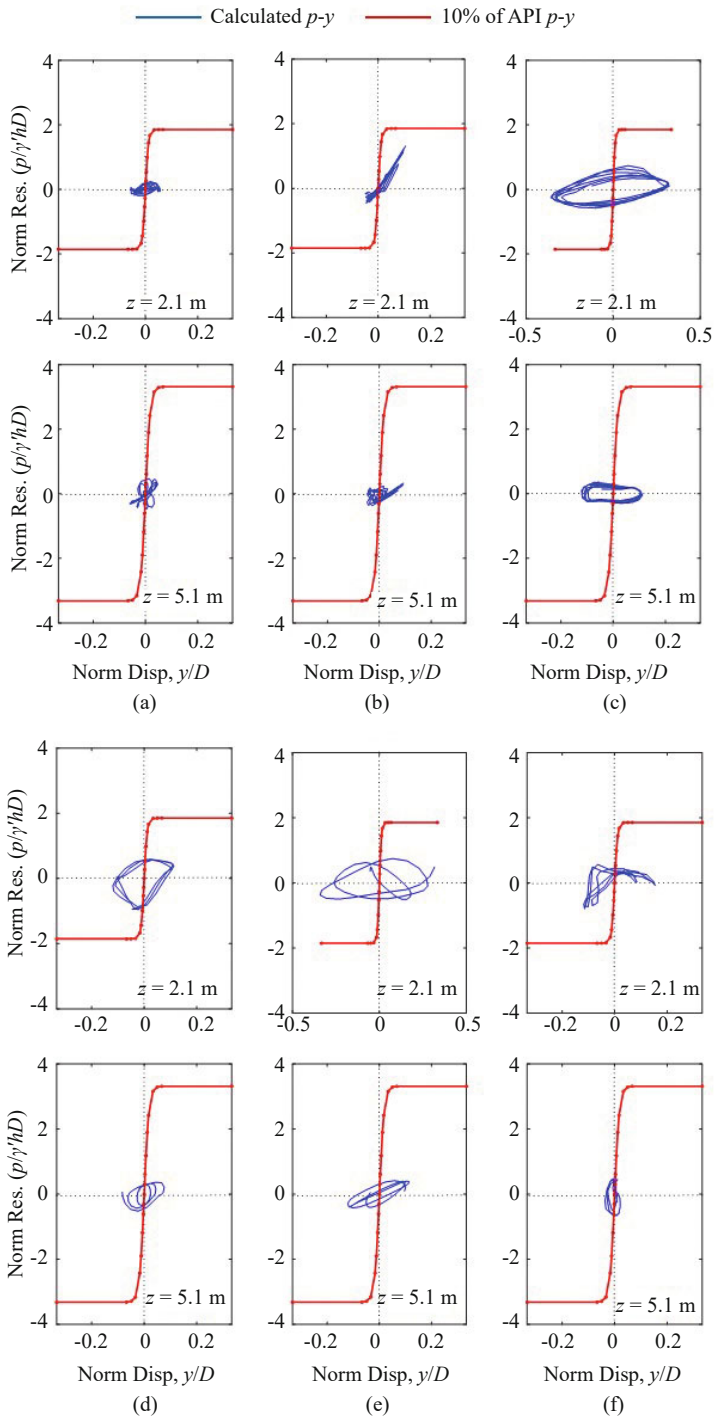

Fig. 7 p-y curves for no lateral spreading cases (a) CT1-A, (b) CT2-A, (c) CT3-A, and for lateral spreading cases (d) CT1-B, (e) CT2-B, (f) CT3-B in fully liquefied soil at two depths and compared with 10% monotonic API p-y curves

soil layer) at the location of strain gauges in the pile. They were also compared with 10% monotonic API *p-y* curves for non-liquefiable soils, marked in red lines in the figure. The difference between the magnitudes of the *p-y* curves in the three cases is mostly due to the distance of the pile group from the quay wall, where CT1-A was 200 mm, CT2-A was 100 mm and CT3-A was 50 mm (in model scale) away from the quay wall. The nearer the quay wall, the higher was the resistance due to the stiff boundary, which can be seen in the figure as a higher magnitude *p-y* curve in CT3-A as compared to the other two *p-y* curves. Although the magnitudes differ for the three cases, it varies in the range of 2% to 6% of the API *p-y* curve for non-liquefied soil.

7.2 *p-y* curves for lateral spreading cases

All other cases except the three discussed in Section 7.1 (i.e., CT1-A, CT2-A and CT3-A) had a free base quay wall, which failed during the test. Figure 8(a) shows the *p-y* curves obtained from CT6-A during the test (0–20 s) at the top, middle and bottom of the liquefied soil layer. As expected, the *p-y* curves calculated are off-centered, which were due to the lateral spreading of the soil as the quay wall failed and the soil experienced a permanent displacement. To obtain a better comparison with the API recommended monotonic *p-y* curves, the lateral spreading component was removed from the soil deformation and the *p-y* curves thus obtained are presented in Fig. 8(b).

The *p-y* curves at the top of the liquefied soil show more resistance (~ 18% of non-liquefied API value) than the *p-y* curves at the bottom part (~ 4% of non-liquefied API value). However, the magnitude of the *p-y* curves should usually be higher at a deeper depth. In the present case, this observation could be due to higher *y* at shallow depth and faster dissipation of excess pore water pressure reducing the degree of liquefaction with an increase in lateral resistance. A similar observation has also been made by Suzuki and Tokimatsu (2004) based on shaking table tests.

Note that the *p-y* curves were back-calculated with some inherent limitations on accuracy due to the limited number of strain measurement points, curve fitting method for bending moment data and soil deformation measurements from acceleration time histories. However, the pattern of the *p-y* curves obtained is reasonably good at the lower level of the liquefied soil layer than at the upper level. One of the reasons may be the inability of filtered accelerometer data to capture the actual displacement in the soil after full liquefaction. The final results for the *p-y* curves are presented at two levels for tests CT1, CT2 and CT3 and at three levels for the other test cases in the liquefied soil layers at the locations of the strain measurement. The *p-y* curves were also compared with the 10% API recommended *p-y* curves for saturated sand at the corresponding depth after removing the drift component. Figures 7(d), 7(e), 7(f), 9 and 10 show the *p-y* curves obtained for the lateral spreading cases at a fully liquefied state (6–8 s). The observation of higher strength but lower stiffness at the top of the liquefied layer than at the bottom of the liquefied layer was consistently observed.

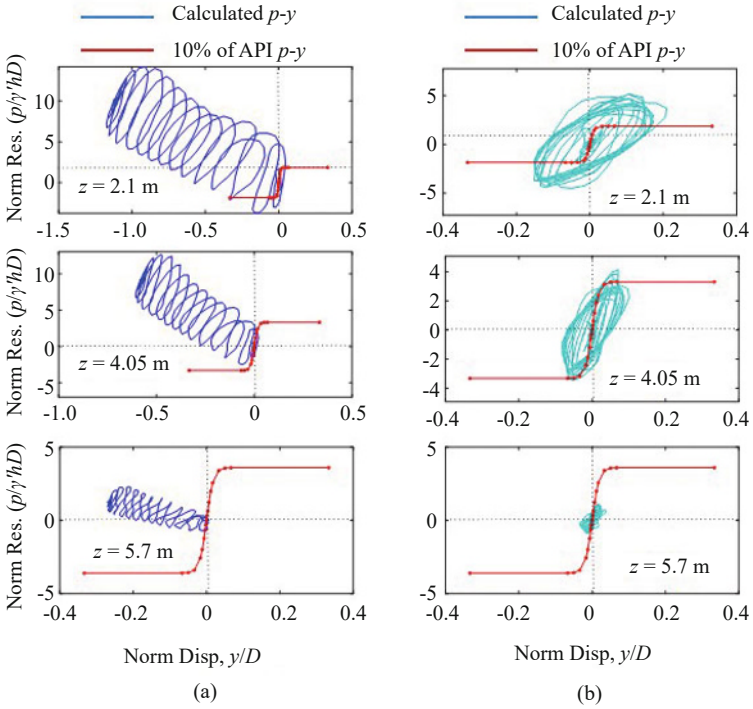

Fig. 8 ***p-y* curve in liquefied soil for CT6-A at three depths, z = 2.1 m, 4.05 m, and 5.7 m, (a) with lateral spreading, and (b) only dynamic component after removing the drift**

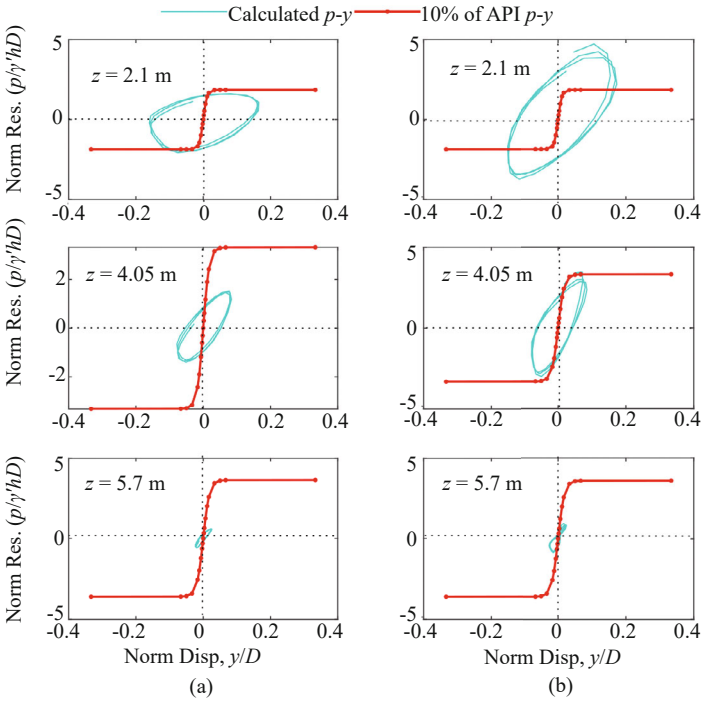

Fig. 9 Back-calculated *p-y* curves for (a) CT5-A and (b) CT-6A in fully liquefied soil at three depths and compared with 10% monotonic API *p-y* curves

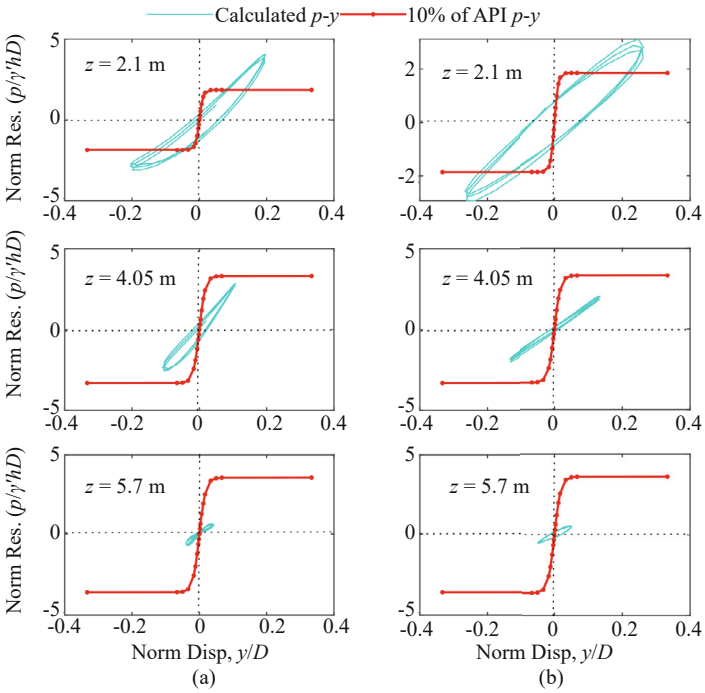

Fig. 10 Back-calculated *p-y* curves for (a) CT7-A and (b) CT8-A in fully liquefied soil at three depths and compared with 10% monotonic API *p-y* curves

7.3 Comparison of the lateral spreading case near to and far from the quay wall

Cases CT4-A and CT4-B were in the test CT4 but the pile groups were positioned at different distances from the quay wall, i.e., CT4-A was at 100 mm away and CT4-B was at 50 mm away (in model scale). Both the pile groups were subjected to lateral spreading due to the failure of the quay wall. The *p-y* curves obtained for both the cases including lateral spreading components are shown in Figs. 11(a) and 11(b). In these cases, as the magnitude of soil movement towards the right was more than the pile movement, the relative pile-soil displacement was negative. Hence, the progression of *p-y* behavior is on the negative side as shown in Figs. 11(a) and 11(b). Comparing the *p-y* curves for both the cases, they are very similar in pattern, but the magnitudes are different at different depths. To get a better comparison of

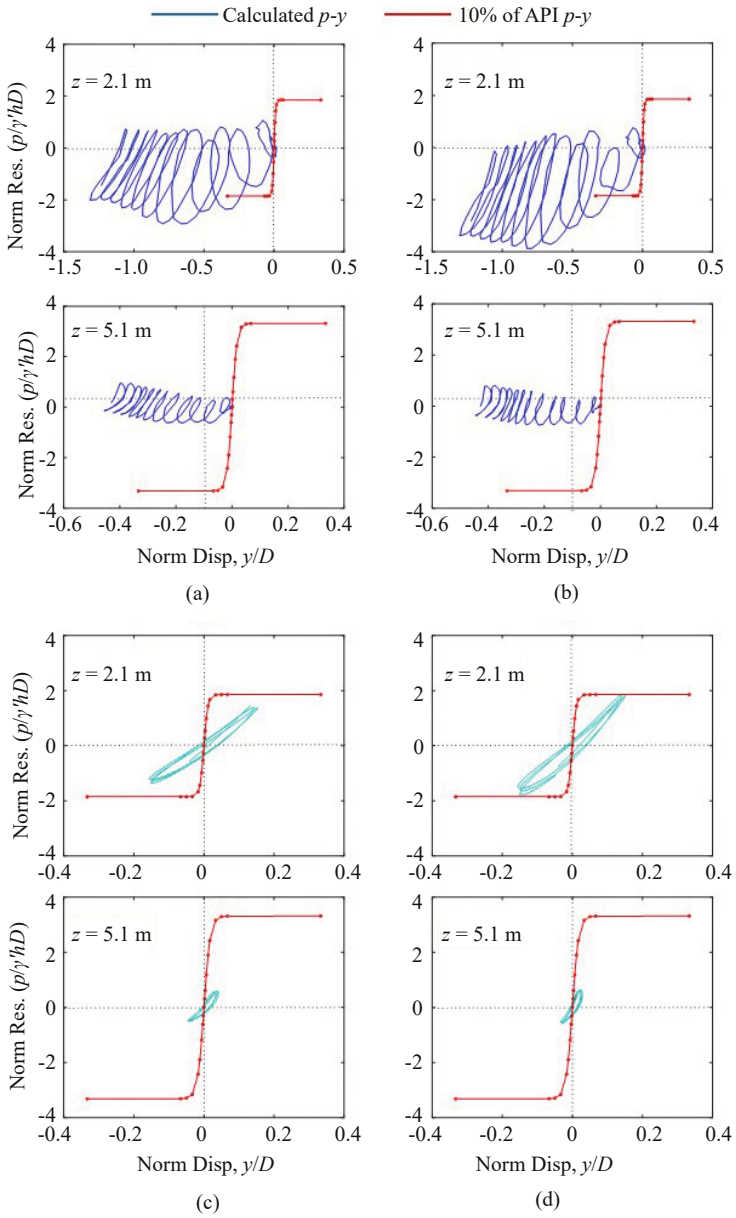

Fig. 11 Back-calculated *p-y* curves for (a) CT4-A and (b) CT4-B subjected to lateral spreading, and (c) CT4-A and (d) CT4-B after removing the lateral spreading component

the magnitudes, the permanent displacement component was removed and the *p-y* curves were plotted as shown in Figs. 11(c) and 11(d). The strength of liquefied soil was found to be about 8%–10% of the API non-liquefied value at the top layer, which reduced to about 2% at the bottom of the liquefied soil layer.

In contrast to the observations made in cases CT1-A, CT2-A and CT3-A with respect to the distance of the non-failing quay wall, the observations in CT4-A and CT4-B do not show any significant difference in results with respect to the distance of the quay wall from the pile group. This could be because in both cases, the quay wall had failed and the influence of a stiff boundary, as present in cases CT1-A, CT2-A, and CT3-A, was absent in CT4-A and CT4-B.

7.4 Comparison of lateral spreading and non-lateral spreading cases under identical test conditions

Tests CT1, CT2 and CT3 had both a lateral spreading (Side-A) and non-lateral spreading (Side-B) model subjected to identical test conditions. The *p-y* curves for CT1-A, CT2-A and CT3A were compared with the *p-y* curves for CT1-B, CT2-B and CT3-B as shown in Fig. 7. The results show no significant change in the pattern and strength of the liquefied soil for these three tests. This suggests that the lateral resistance exerted on the pile was either due to the flow of liquefied soil or that the deflection of the pile in non-flowing liquefied soil was about the same.

8 Summary of conclusions and outlook

Twelve pile group results from centrifuge tests have been investigated in this study. The *p-y* curves have been back-calculated from the recoded bending strain of the pile and the soil acceleration data. Regardless of the limitations in the numerical analysis procedure used in this study, the analyses results show reduced resistance of liquefied soil, as expected. From the above study, the following conclusions can be made.

- The back-calculated *p-y* curve shape and magnitude was relatively consistent across the tests for a particular depth of consideration, which provides confidence with regard to the repeatability of the observations.
- The *p-y* curves can be characterised by low initial stiffness and ultimate strength. Some of the present tests have shown nearly undrained behavior for *p-y* curves in liquefied soils, where the initial stiffness of the *p-y* curves was very low and it increased with the increase in pile-soil displacement. However, the conventional practice overestimated the initial stiffness of the *p-y* curves in liquefied soil.
- Results from all the test cases showed that the lateral resistance of loose to medium dense soil (relative density ≈ 50% in this study) can normally range from 1%-10% of the API suggested value for non-liquefied soil. This is with the consideration of a mean and more representative value of lateral resistance at the middle of the liquefied soil layer.
- In some cases, the results at the top of the liquefied soil layer were influenced by the overlaying non-liquefied soil layer that showed larger resistance when compared to other cases. At some instances, it was about 18% larger than that of the API suggested value for nonliquefied soil. This higher resistance could also be due to larger relative pile-soil displacement at shallow depth due to faster excess pore water pressure dissipation and the development of the wedge mechanism of failure.
- Comparison between lateral spreading and non-lateral spreading ground in liquefied soil showed that, the strength of liquefied soil did not change in the lateral spreading of the liquefied soil case than that in the case of deflection of the pile in nonspreading liquefied soil. These two cases of the *p-y* curves are differentiated in literature as (a) lateral spreading case where the soil flows past the pile, and (b) non-lateral spreading case where the pile vibrates in liquefiable soil. As per the authors′ knowledge, this is the first set of tests that directly compares lateral spreading and non-lateral spreading cases under identical test conditions.

8.1 Translation of model test results to the construction of *p-y* curves for use in practice

One of the main reasons to carry out model tests is to verify hypotheses, conjectures, mechanisms and processes that control the behavior of interest. The scaled model tests showed that liquefied soil has very low stiffness for small amplitude strains, which are in alignment with other tests such as pulling a pipe in initially liquefied soil (i.e., see Dash, 2010). The practical implication is that the *p-y* curves have an upwards concave shape (i.e., strain hardening behavior), which differs drastically from the standard *p-y* curves used in practice (see Fig. 1 for a comparison of the shapes). However, the challenge is to develop *p-y* curves for practical use from these scaled model tests. The sand used in scaled model tests is laboratory clean sand, which differs greatly from the sand at the site, not only due to layering and cementation but also to index properties, including particle size distribution. Therefore, it is prudent to develop a *p-y* curve based on soil element test results from actual samples from a given site using readily available apparatus. Readers are referred to the element tests of liquefied soil available in Lombardi *et al.* (2014, 2017) and Rouhalamin *et al.* (2017), where multi-stage triaxial tests were carried out to identify the parameters necessary to construct the *p-y* curve. A practical method to construct a mechanics-based *p-y* curve of liquefied soil based on the understanding gained from the scaled model tests presented herein and soil element tests is available in Dash *et al.* (2017), together with an explanatory example. This newly developed *p-y* curve has also been used in the work of Zhang *et al.* (2020).

Acknowledgment

The first author acknowledges the financial support provided by UKIERI to carry out this research work at the University of Oxford. The authors also thank Prof. Anthony Blakeborough of the University of Oxford for providing guidance for some of the analyses presented herein. The authors also thank Dr. T. Tazoh, Japan, and Dr. J. H Jang, Korea for providing the experimental data used in this analysis.

References

AIJ (2001), "Recommendations for Design of Building Foundations," *Architectural Institute of Japan*, Japan.

API (2014), "Recommended Practice for Planning, Designing, and Constructing Fixed Off-shore Platforms - Working Stress Design," *American Petroleum Institute*, USA.

Brandenberg SJ (2005), "Behavior of Pile Foundations in Liquefied and Laterally Spreading Ground," *PhD Thesis*, Univ. of California at Davis, Davis, California.

Bouzid DJ, Bhattacharya S and Dash SR (2013), "Winkler Springs (*p-y* Curves) for Pile Design from Stress-Strain of Soils: FE Assessment of Scaling Coefficients Using the Mobilized Strength Design Concept," *Geomechanics and Engineering*, **5**(5): 379–399.

Bhattacharya S, Orense RP and Lombardi D (2019), "Seismic Design of Foundations: Concepts and Applications," ICE Publishing.

Chanerley AA and Alexander NA (2007) "Correcting Data from an Unknown Accelerometer Using Recursive Least Squares and Wavelet De-Noising," *Computers and Structures*, **85**(21-22): 1679–1692.

Dash SR, Bhattacharya S, Blakeborough A and Hyodo M (2008), "*p-y* Curve to Model Lateral Response of Pile Foundations in Liquefiable Soils," *14th World Conference on Earthquake Engineering* (14WCEE), October 12-17, 2008, Beijing, China.

Dash (2010), Lateral Pile Soil Interaction in Liquefiable Soils, *PhD Thesis*, University of Oxford.

Dash SR, Rouholamin M, Lombardi D and Bhattacharya S (2017), "A Practical Method for Construction of *p-y* Curves for Liquefiable Soils," *Soil Dynamics and Earthquake Engineering*, **97**: 478–481.

Dou H and Byrne PM (1996), "Dynamic Response of Single Piles and Soil–Pile Interaction," *Canadian Geotechnical Journal*, **33**(1): 80–96.

Finn WDL (2005), "A Study of Piles during Earthquakes: Issues of Design and Analysis," *Bulletin of Earthquake Engineering*, **3**: 141–234. https://doi.org/10.1007/s10518-005-1241-3

Gerolymos1 N, Escoffier S, Gazetas G and Garnier J (2009), "Numerical Modeling of Centrifuge Cyclic Lateral Pile Load Experiments," *Earthquake Engineering and Engineering Vibration*, **8**(1): 61–76.

Han S (2003), "Retrieving the Time History of Displacement from Measured Acceleration Signal," *Journal of Mechanical Science and Technology*, **17**(2): 197–206.

Jeanjean P (2009), "Re-Assessment of *p-y* Curves for Soft Clays from Centrifuge Testing and Finite Element Modeling," *Offshore Technology Conference*.

Janalizadeh A and Zahmatkesh (2015), "A Lateral Response of Foundations in Liquefiable Soils," *Journal of Rock Mechanics and Geotechnical Engineering*, 7(5): 532–539.

JRA (2002), "Specifications for Highway Bridges, Part V. Seismic Design," *Japanese Road Association*, Tokyo, Japan.

Lombardi D, Dash SR, Bhattacharya S, Ibraim E, Wood DM and Taylor CA (2017), "Construction of Simplified Design *p-y* Curves for Liquefied Soils," *Geotechnique*, **67**(3): 216–227.

Lombardi D, Bhattacharya S, Hyodo M and Kaneko T (2014), "Undrained Behavior of Two Silica Sands and Practical Implications for Modelling SSI in Liquefiable Soils," *Soil Dynamics and Earthquake Engineering*, **66**: 293–304.

Madabhushi G, Knappett J and Haigh S (2009), "Design of Pile Foundations in Liquefiable Soils," *Imperial College Press*, 1 Edition, ISBN-13: 978-1848163621.

Matlock H and Ripperger EA (1956), "Procedures and Instrumentation for Tests on a Laterally Loaded Pile," *Proceedings of Eighth Texas Conference on Soil Mechanics and Foundation Engineering*.

Mohanty P, Dan X, Biswal S and Bhattacharya S (2021), "A Shake Table Investigation of Dynamic Behavior of Pile Supported Bridges in Liquefiable Soil Deposits," *Earthquake Engineering and Engineering Vibration*, **20**(1): 1–24.

Park KT, Kim SH, Park HS and Lee KW (2005), "The Determination of Bridge Displacement Using Measured Acceleration," *Engineering Structures*, **27**(3): 371–378.

Rollins KM, Gerber TM, Lane JD and Ashford SA (2005), "Lateral Resistance of a Full-Scale Pile Group in Liquefied Sand," *Journal of Geotechnical and Geoenvironmental Engineering*, **131**: 115–125.

Rouholamin M, Bhattacharya S and Orense RP (2017), "Effect of Initial Relative Density on the Post-Liquefaction Behavior of Sand," *Soil Dynamics and Earthquake Engineering*, **97**: 25–36.

Sato M (1994), "A New Dynamic Geotechnical Centrifuge and Performance of Shaking Table Tests," In: *Proc. Centrifuge 94*, Leung, Lee and Tan (eds), Balkema, Rotterdam, ISBN 9054103523.

Suzuki H and Tokimatsu K (2004), "Pore Water Pressure Response Around Pile and Its Effects on *p-y* Relation During Liquefaction," *Proceedings of the First International Conference of Urban Earthquake Engineering* (*CUEE*)*, Mar 8-9, Tokyo Institute of Technology*, Tokyo Tech, Japan, 493–499.

Tazoh T, Sato M, Jang J and Gazetas G (2008), "Centrifuge Tests on Pile Foundation-Structure Systems affected by Liquefaction-Induced Soil Flow After Quay Wall Failure," *Proceedings of the 14th World Conference on Earthquake Engineering*, October 12-17, 2008, Beijing, China.

Thavaraj T, Liam Finn WD and Wu G (2010), "Seismic Response Analysis of Pile Foundations," *Geotechnical and Geological Engineering*, **28**(3): 275–286.

Wilson DW (1998), "Soil-Pile-Superstructure Interaction in Liquefying Sand and Soft Clay," *PhD Thesis*, University of California, Davis, USA.

Wilson DW, Boulanger RW and Kutter BL (2000), "Observed Seismic Lateral Resistance of Liquefying Sand," *Journal of Geotechnical Engineering*, ASCE, **126**(10): 898–906.

Zhang XA and Yang ZJ (2018), "Numerical Analyses of Pile Performance in Laterally Spreading Frozen Ground Crust Overlying Liquefiable Soils," *Earthquake Engineering and Engineering Vibration*, **17**(3): 491–499.

Zhang X, Tang L, Ling X and Chan A (2020), "Critical Buckling Load of Pile in Liquefied Soil," *Soil Dynamics and Earthquake Engineering*, **135**: 106197.